Journal of Korean Society of
Coastal and Ocean Engineers
Vol. 9, No. 1, pp. 9~23, March 1997

Two Layer Modelling with Applications to Exchange Flow and Internal Tide
이층류 모델링의 교환류와 내부조석파 연구에의 적용

Sok Kuh Kang*, Michael B. Abbott*, Heung-Jae Lie***, Ki-Dai Yum* and Jae-Kwi So*
강석구* · 마이클 아보트** · 이흥재*** · 염기대* · 소재귀*

Abstract □ A numerical study of a two-layer, stratified flow is investigated, using the implicit finite difference method in one dimension. The results of computational method have been tested and, in case of lock exchange flow, compared with the results of experimental data. The results of model experiments with various interfacial, bottom friction coefficients along with various time weighting factor of numerical scheme and dissipative interface are shown and discussed. Two-layer model experiment has been also carried out to investigate the generation and propagation characteristics of internal tidal wave over the steep bottom topography under stratified condition. The internal wave seems to well radiate through the downstream boundary under the experiments adopting radiation conditions both at two layers and only at upper layer, confirming the applicability of radiational boundary condition in stratified flows. It is also shown that the internal wave through the downstream boundary propagates more actively with increasing thickness of lower layer in the downstream. This implies that the potential tidal energy in the interface will depend upon the thickness of lower layer for the constant thickness of upper layer.

Keywords : two layer modeling, exchange flow, internal tidal wave, radiational boundary condition, time weighting factor, stratified flow

要　旨 : 一次元 2層 成層流에 대한 陰解 有限差分法을 이용한 數値實驗 연구를 실시하였다. 수치방법에 대한 기본 테스트와 함께 水理實驗 자료가 있는 交換流에 대한 모델결과의 검증을 실시하였다. 다양한 層間 및 해저마찰계수와 수치계산의 시간 加重因子, smoothing 인자에 대한 모델 반응 결과를 제시한다. 아울러 2층 모델을, 成層이 되어 있고 海底面 기울기가 급격한 조건에서 內部波의 발생과 전파 특성에 대한 연구에 응용하였다. 하류부 경계의 1개 층 혹은 2개 층을 放射條件으로 처리했을 때, 下流部를 통해 내부파가 잘 전파되어, 방사파 조건의 成層流 모델링에의 적용성을 확인하였다. 또한 하류부의 저층두께가 두꺼울수록 내부파가 하류부 경계를 통해 활발히 전파해 가는 것으로 나타났다. 이는 層間의 내부파 위치에너지는 上層의 두께가 일정한 경우, 下層의 두께에 좌우될 것임을 암시한다.

핵심용어 : 2층류 모델링, 교환류, 내부 조석파, 방사 경계조건, 시간 가중인자, 성층류

1. INTRODUCTION

Stratified flow is a common phenomena in estuaries, lakes and oceans. In case of estuaries the stratification is induced mainly by salinity difference between fresh and salt waters and such stratification is incorporated with tidal variation to often form an oscillating salt wedge which is closely related to shoaling phenomena.

*한국해양연구소 연안공학부 (Coastal Engineering Division, Korea Ocean Research and Development Institute, Ansan P.O. Box 29, 425-600, Korea)
**델프트 국제수리환경공학연구소 (International Institute of Hydraulic and Environmental Engineering, Delft, The Netherlands)
***한국해양연구소 해양물리연구부 (Physical Oceanography Division, Korea Ocean Research and Development Institute, Ansan P. O. Box 29, 425-600, Korea)

In lakes stratification or stratified flow occurs due to daily or seasonal temperature variation of atmosphere and also it occurs by cooling water discharged from power plant. In oceans they exist when water masses of different origins meet each other. On a large scale density variation in oceans happens mainly due to unbalanced solar radiation whose quantity varies according to latitude. Local stratification could also occur by thermal discharge or accidental oil spreading. In addition to stratified flow of water the behavior of front between air and warm air in atmosphere could be treated as a stratified flow. Due to its importance both from theoretical and practical points of view this problem has been one of the extensively studied topics in fluid mechanics.

When we try to solve the stratified flow problem numerically two approach methods are available. one is the traditional layer approach method and the other is the method to use turbulence level model. Compared with level model, the layer model has more advantage to examine the physics of stratified flows. About the numerical scheme, previously computational models in one dimension using explicit scheme were introduced by Vreugdenhil (1970) and Hodgins *et al.* (1977). An implicit scheme was described by Abbott and Grubert (1972) and Hodgins (1979) to treat a two-layer equation. In case of using explicit scheme the major computational problem is related to numerical stability. Due to the great difference of velocity of propagation of external and internal waves, which is often case in nature, it is required to decouple the original coupled equations to set up a reasonable computation for the internal modes, as noticed by Vreugdenhil (1970). Explicit scheme becomes, however, impractical for simulation in deep water. Implicit scheme overcomes this stability restriction and it can use coupled flow equation as a governing equation. The main restriction of implicit scheme in this aspect is considered only for the purpose of increasing the numerical accuracy. With these several other considerations, noted by Abbott (1972), lead to the use of an implicit scheme.

In this paper the development of two layer model in one dimension is described in order to investigate the phenomena related to stratified flows, especially with applications to exchange flow modelling and the fundamental investigation for the generation and propagation of internal tide over the steep bottom topography occurring in the shelf break region such as in the East China Sea. The numerical method based upon the extension of Abbott and Ionescu (1967) scheme was adopted in order to solve the coupled equation system of the two layer flow. The developed model is initially verified against the laboratory experimental data available for the exchange flow. The applicability of radiational boundary condition was also examined for the layer model.

2. THEORETICAL DESCRIPTION

2.1 Governing Equations

A two-layer stratified nearly horizontal flow is considered in terms of the definition sketch, the lower layer as is shown in Fig. 1, in which subscripts 0 is used to indicate the lower layer. u and u_0, indicate upper and lower layer velocity, respectively, and p, p_0 denote volume flux at each layer.

A mass flux, w_0, leaves the bottom fluid to enter the top fluid. In addition to the usual wind stress τ_w and bottom stress τ_b, an interfacial stress τ_i is also introduced. There are extensive literatures on these exchange and shear stress (Abraham and Eysink, 1971; Ellison and Turner, 1959). This entrainment effect was assumed to be zero in real calculation. The following conservation laws may then be written following Abbott (1979).

Conservation of mass:

$$\frac{\partial}{\partial t}(\rho h)+\frac{\partial}{\partial x}(\rho u h)-(\rho_0 w_0-\rho w)=0 \tag{1}$$

$$\frac{\partial}{\partial t}(\rho_0 h_0)+\frac{\partial}{\partial x}(\rho_0 u_0 h_0)-(\rho w-\rho_0 w_0)=0 \tag{2}$$

Conservation of momentum:

$$\frac{\partial}{\partial t}(\rho_0 u_0 h_0)+\frac{\partial}{\partial x}(\rho_0 u_0^2 h_0)$$
$$+gh_0\left[\frac{\partial}{\partial x}(\rho h)+\rho_0\frac{\partial}{\partial x}(h_0+Z)+\frac{h_0}{2}\frac{\partial \rho_0}{\partial x}\right]$$

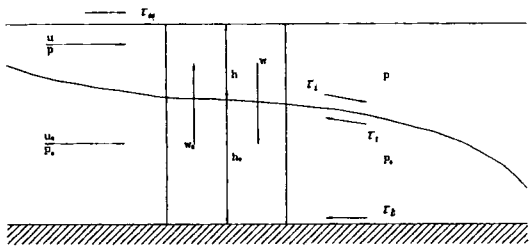

Fig. 1. Definition sketch for a stratified flow.

$$-(\rho uw - \rho_0 u_0 w_0) + (\tau_b - \tau_i) = 0 \tag{3}$$

$$\frac{\partial}{\partial t}(\rho uh) + \frac{\partial}{\partial x}(\rho u^2 h) + gh\rho\frac{\partial}{\partial x}(h + h_0 + Z) + \frac{gh^2}{2}\frac{\partial \rho}{\partial x} + (\rho uw - \rho_0 u_0 w_0) + (\tau_i - t_w) = 0 \tag{4}$$

In the above equations several physical processes were introduced. Exchange of fluid across the interface, with w_0 crossing from the lower to upper layer and w crossing the upper to the lower layer, as schematized in Fig. 1. These exchange may take the full density of their initiating layer across to their receiving layer, or they may work with only a reduced part of the density difference. In equation of motion an interfacial stress was introduced. as well as wind stress, and bottom stress. It is seen that in the absence of interfacial mass transfers, both Eq. (1) and Eq. (2) retain the conservation form, individually. Their sum, corresponding to a mass balance over the total fluid, provides also a conservation. It is seen that if ρ and ρ_0 are constant in each layer, Eqs. (1) to (4) reduce to

$$\frac{\partial h}{\partial t} + \frac{\partial}{\partial x}(uh) - (\frac{\rho_0}{\rho}w_0 - w) = 0 \tag{5}$$

$$\frac{\partial h_0}{\partial t} + \frac{\partial}{\partial x}(u_0 h_0) - (\frac{\rho}{\rho_0}w - w_0) = 0 \tag{6}$$

$$\frac{\partial}{\partial t}(u_0 h_0) + \frac{\partial}{\partial x}(u_0^2 h_0) + gh_0\frac{\partial}{\partial x}(h_0 + \lambda h + Z) - (\lambda uw - u_0 w_0) + (\tau_b - \tau_i)/\rho_0 = 0 \tag{7}$$

$$\frac{\partial}{\partial t}(uh) + \frac{\partial}{\partial x}(u^2 h) + gh\frac{\partial}{\partial x}(h_0 + h + Z) + (uw - \lambda u_0 w_0) (\tau_i - \tau_w)/\rho = 0 \tag{8}$$

The two-layer system is closed with the scalar conservation equations:

$$\frac{\partial \rho}{\partial t} + u\frac{\partial \rho}{\partial x} - D\frac{\partial^2 \rho}{\partial x^2} - \frac{w_0}{h}(\rho_0 - \rho) = 0 \tag{9}$$

$$\frac{\partial \rho_0}{\partial t} + u_0\frac{\partial \rho_0}{\partial x} - D\frac{\partial^2 \rho_0}{\partial x^2} - \frac{w}{h_0}(\rho - \rho ub\,0) = 0 \tag{10}$$

or in the form

$$\frac{\partial g}{\partial t} + A\frac{\partial g}{\partial x} = C \tag{11}$$

in which

$$g = \begin{bmatrix}\rho \\ \rho_0\end{bmatrix}, A = \begin{bmatrix}u \\ u_0\end{bmatrix}, C = \begin{bmatrix} D\frac{\partial^2 \rho}{\partial x^2} + \frac{w_0}{h}(\rho_0 - \rho) \\ D\frac{\partial^2 \rho_0}{\partial x^2} + \frac{w}{h_0}(\rho - \rho_0)\end{bmatrix} \tag{12}$$

In Eqs. (9) and (10) the density variation in each layer is shown to be due to advective, diffusive processes within each layer and mixing effect between layers.

Both from the computational and analytical point of view it is sometimes required that the governing equation system be simplified or take alternative form. We proceed to consider the characteristics of physical system. When all exchanges, stresses and bed variation are excluded and the time and spatial variations of density in each layer are neglected, the Eqs. (5), (6), (7), (8) reduce to

$$\frac{\partial h}{\partial t} + u\frac{\partial h}{\partial x} + h\frac{\partial u}{\partial x} = 0 \tag{13}$$

$$\frac{\partial h_0}{\partial t} + u_0\frac{\partial h_0}{\partial x} + h_0\frac{\partial u_0}{\partial x} = 0 \tag{14}$$

$$\frac{\partial u}{\partial t} + u\frac{\partial u}{\partial x} + g\frac{\partial h}{\partial x} + g\frac{\partial h_0}{\partial x} = 0 \tag{15}$$

$$\frac{\partial u_0}{\partial t} + u_0\frac{\partial u_0}{\partial x} + g\lambda\frac{\partial h}{\partial x} + g\frac{\partial h_0}{\partial x} = 0 \tag{16}$$

The equation system (13) to (16), with equations of variation, gives the equivalent matrix system as (Abbott, 1979)

$$\begin{bmatrix} 1 & u_0 & 0 & h_0 & 0 & 0 & 0 & 0 \\ 0 & g & 1 & u_0 & 0 & \lambda g & 0 & 0 \\ 0 & 0 & 0 & 0 & 1 & u & 0 & h \\ 0 & g & 0 & 0 & 0 & g & 1 & u \\ dt & dx & 0 & 0 & 0 & 0 & 0 & 0 \\ 0 & 0 & dt & dx & 0 & 0 & 0 & 0 \\ 0 & 0 & 0 & 0 & dt & dx & 0 & 0 \\ 0 & 0 & 0 & 0 & 0 & 0 & dt & dx \end{bmatrix} \begin{bmatrix} \partial h_0/\partial t \\ \partial h_0/\partial x \\ \partial u_0/\partial t \\ \partial u_0/\partial x \\ \partial h/\partial t \\ \partial h/\partial x \\ \partial u/\partial t \\ \partial u/\partial x \end{bmatrix} = \begin{bmatrix} 0 \\ 0 \\ 0 \\ 0 \\ dh_0 \\ du_0 \\ dh \\ du \end{bmatrix} \tag{17}$$

Then, equating the determinant of the coefficient matrix to zero, we obtain the condition that the vector of derivatives be indeterminate

$$\begin{bmatrix} u_0-\dot{x} & h_0 & 0 & 0 \\ g & u_0-\dot{x} & \lambda g & 0 \\ 0 & 0 & u-\dot{x} & h \\ g & 0 & g & u-\dot{x} \end{bmatrix} \tag{18}$$

where $\dot{x} = dx/dt$ are then the characteristic directions. Writing out the determinant gives the characteristic equation

$$[(u_0-\dot{x})^2 - gh_0][(u-\dot{x})^2 - gh] - \lambda g^2 h_0 h = 0 \tag{19}$$

A graphical method to investigate Eq. (19) was described by Abbott and Torbe (1963). The approximate solution of Eq. (19) is given in Vreugdenhil (1970) as follows:

$$\dot{x}_{1,2} = \frac{uh + u_0 h_0}{h + h_0} \pm [g(h + h_0)]^{1/2} \tag{20}$$

$$\dot{x}_{3,4} = \frac{uh_0 + u_0 h}{h + h_0} \pm \left[\frac{g(1-\lambda)hh_0}{h + h_0} - \frac{(u-u_0)^2 hh_0}{(h + h_0)^2}\right]^{1/2} \tag{21}$$

with some assumption. $x_{1,2}$ and $x_{3,4}$ agree with the celerities of long surface wave and a long internal wave, respectively. The order of magnitude of $\dot{x}_{1,2}$ and $\dot{x}_{3,4}$ is determined by square roots as follows:

$$\frac{\dot{x}_{3,4}}{\dot{x}_{1,2}} \sim \left[\frac{(1-\lambda)hh_0}{(h + h_0^2)} - \frac{(u-u_0)^2 hh_0}{g(h + h_0)^3}\right]^{1/2} \tag{22}$$

For usual sea water the order of magnitude will be 10^{-1}~ 10^{-2}

2.2 Data Structure and Boundary Condition

As mentioned by Abbott (1961, 1963), the characteristics are associated in pairs such that each pair appertains to a fluid layer of the system, then it can be said that when two of the characteristics associated with any layer have the same sign, then the flow in that layer is a supercritical flow, while when these signs are different it is a subcritical flow. With this convention the five basic characteristic structure, as shown in Fig. 2, can be explained.

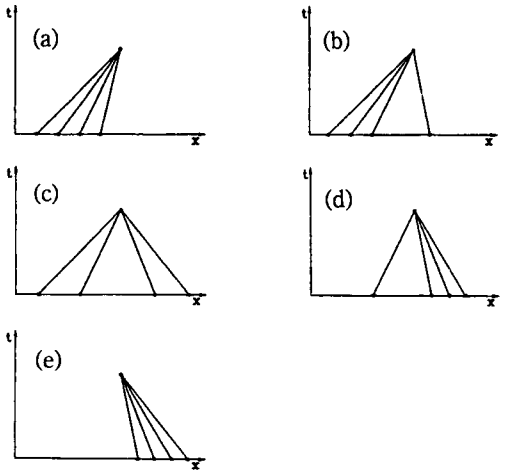

Fig. 2. Five data structure of characteristics for two-layer flow (Abbott, 1979).

From the method of characteristics (Abbott, 1963) it is shown that the number of data points presented at a boundary equals the number of characteristics initiated from any point of that boundary, so Fig. 2(a) would require four-point left boundary data and zero-point right boundary data. Fig. 2(c) would require two point left boundary data and two point right boundary data, and so on. But it is seen that it is not only necessary to present, the correct number of data points at each boundary, but it is also necessary to present these in the correct place. For the limiting case details are given (Abbott, 1961 and 1972).

In this study the range is restricted only to the data structure shown in Fig. 2(c), that is, subcritical-subcritical case. it means that it is required to give both left and right boundary two data with one data to upper layer and one data to the lower layer in each side. In fact it is seen that the two-layer fluid is seen to possess five characteristic structure and nine data structures, although in practical case only five appear to be of interest of the latter.

3. DISCRETE APPROXIMATION OF CONTINUOUS FORMS

The selection of a particular finite scheme to solve

any of the equation systems numerically determines the space-time distribution of the dependent variables. In this study to solve two-layer flow numerically the physical system is simplified. That is, the study is restricted to consider the flow per unit span width in a channel of uniform depth with interfacial and bottom stresses, but without vertical turbulent mixing and longitudinal stress. In spite of this simplification we can still study many essential aspects of two-layer system from both physical and numerical point of views, through a appropriate simulation.

With interfacial and bottom stresses the Eqs. (1) to (4) can be written in the algorithm form as follows:

$$M_1\frac{\partial f}{\partial t}+M_2\frac{\partial f}{\partial t}+M_3\frac{\partial f}{\partial x}=S \tag{23}$$

where $M_1=I$, the identity matrix and

$$f=\begin{bmatrix} h \\ h_0 \\ p \\ p_0 \end{bmatrix}, S=\begin{bmatrix} 0 \\ 0 \\ \frac{\tau_w}{\rho}-\frac{\tau_i}{\rho_0} \\ \frac{\tau_i}{\rho_0}-\frac{\tau_b}{\rho_0} \end{bmatrix}$$

$$M_2=\begin{bmatrix} 0 & 0 & 0 & 0 \\ 0 & 0 & 0 & 0 \\ -\frac{2p}{h} & 0 & 0 & 0 \\ 0 & -\frac{2p_0}{h_0} & 0 & 0 \end{bmatrix}, M_3=\begin{bmatrix} 0 & 0 & 1 & 0 \\ 0 & 0 & 0 & 1 \\ gh-\frac{p^2}{h^2} & gh & 0 & 0 \\ gh_0\lambda & gh_0-\frac{p_0^2}{h_0^2} & 0 & 0 \end{bmatrix}$$

And in this case the transport-diffusion equation is written as follows:

$$\frac{\partial f}{\partial t}+M\frac{\partial f}{\partial x}=S \tag{24}$$

where

$$f=\begin{bmatrix} \rho \\ \rho_0 \end{bmatrix}, M=\begin{bmatrix} \frac{p}{h} & 0 \\ 0 & \frac{p_0}{h_0} \end{bmatrix}, S=\begin{bmatrix} D\frac{\partial^2\rho}{\partial x^2} \\ D\frac{\partial^2\rho_0}{\partial x^2} \end{bmatrix}$$

In the above simplified situation the density effect appears in the dynamic equation only as a constant λ. So, even though there is no vertical mixing between two layers, at least the time or spatial variation of density in each layer is required for this transport diffusion equation to have more than symbolic form.

3.1 The System of Discrete Approximation

The difference method introduced by Abbott and Ionescu is generalized to the coupled two-layer equations. The implicit discrete operator with space-staggered dependent variables can be defined. j is grid number, and θ defined as a forward time weighting. Then in finite difference form the finite difference equations only for the continuity and momentum equations of upper layer become.

$$\frac{h_j^{n+1}-h_j^n}{\Delta t}+\left[\theta\frac{p_{j+1}^{n+1}-p_{j-1}^{n+1}}{2\Delta x}+(1-0)\frac{p_{j+1}^n-p_{j-1}^n}{2\Delta x}\right]=0 \tag{25}$$

$$\begin{aligned}&\frac{p_j^{n+1}-p_j^n}{\Delta t}-\frac{2p}{h}\left[\frac{h_{j+1}^{n+1}-h_{j+1}^n}{2\Delta x}+\frac{h_{j-1}^{n+1}-h_{j-1}^n}{2\Delta x}\right]\\&+(gh-\frac{p^2}{h^2})\left[\frac{h_{j+1}^{n+1}-h_{j-1}^{n+1}}{2\Delta x}+(1-0)\frac{h_{j+1}^n-h_{j-1}^n}{2\Delta x}\right]\\&+gh\left[\theta\frac{h_{0j+1}^{n+1}-h_{0j-1}^{n+1}}{2\Delta x}+(1-\theta)\frac{h_{0j+1}^n-h_{j-1}^n}{2\Delta x}\right]=\tau_i/\rho\end{aligned} \tag{26}$$

The finite difference form for the equations of lower layer can be obtained in a similar manner to those of upper layer. Each equation of the finite difference equations can be rearranged to take the form

$$\begin{aligned}&A_{i,j}h_{j-1}+B_{i,j}h_{0j-1}+C_{i,j}p_j+D_{i,j}p_{0j}\\&+E_{i,j}h_{j+1}+F_{i,j}h_{0j+1}=G_{i,j}\end{aligned} \tag{27}$$

where i=1,2,3,4 denote difference equations corresponding to continuity equations of upper and lower layers and momentum equations of upper and lower layers, respectively and j, grid point.

The expression of stresses in finite difference form requires care. According to the numerical study (Abbott and Verghoog, 1968) the following form is necessary for computational stability. With a linear relation for the interfacial stress

$$\frac{\tau_i}{\rho}=k_i(u-u_0)\Delta Z^{-1},\ \Delta Z=(h+h_0)/2 \tag{28}$$

the difference form is

$$\frac{\tau_1}{\rho}=\frac{k_i\theta}{\Delta Z^{n+1}}\left(\frac{p_j^{n+1}}{h_j^{n+1}}-\frac{p_{0j}^{n+1}}{h_{0j}^{n+1}}\right)+\frac{k_i(1-\theta)}{\Delta Z^{n}}\left(\frac{p_j^{n}}{h_j^{n}}-\frac{p_{0j}^{n}}{h_{0j}^{n}}\right) \tag{29}$$

And with a relation for the bottom stress

$$\frac{\tau_b}{\rho_0}=k_b\,u_0|u_0| \tag{30}$$

the difference form is

$$\tau_b=\theta k_b\,\rho_0^{n+1}\left(\frac{p_0}{h_0}\right)^{n+1}\left|\frac{p_0}{h_0}\right|^{n+1}+(1-0)k_b\,\rho_0^{n}\left(\frac{p_0}{h_0}\right)^{n}\left|\frac{p_0}{h_0}\right|^{n} \tag{31}$$

with these forms the coefficients of Eq. (27) have their explicit forms.

The truncation error of the finite difference form can be simply obtained in a sense of Taylors series expansion about the centering point. Then it is seen that the difference equation system are unconditionally consistent with the continuous system of Eq. (23). The order of truncation error is $O(\Delta t, \Delta x^2)$. But when $\theta = 0.5$ the odd order term in Δt cancel and reduce to $O(\Delta t, \Delta x^2)$. That is, the truncation error in Eq. (26) in time, $E(t)$, is

$$E(t)=\frac{1}{2!}\frac{\partial^2 h}{\partial t^2}\Delta t\,[(1-\theta)^2-\theta^2]+0(\Delta t^2) \tag{32}$$

so $E(t)$ reduces to $O(\Delta t^2)$ for $\theta = 0.5$

The solution at $(n+1)\Delta t$ of these four equations converge to solving 6 band width matrix in the corresponding set of algebraic equations. The system of algebraic equations have the structure to be solved by double sweep method.

3.2 Stability Analysis

The linear stability analysis of discrete equation system is made using the Von Neumanns method.

Let

$$p_j^n=\sum_k \xi_{1,k}^n \exp(ikmj\Delta x)$$

$$h_j^n=\sum_k \xi_{2,k}^n \exp(ikmj\Delta x)$$

$$p_{0j}^n=\sum_k \xi_{3,k}^n \exp(ikmj\Delta x)$$

$$h_{0j}^n=\sum_k \xi_{4,k}^n \exp(ikmj\Delta x) \tag{33}$$

Then the difference equation system for certain wave component provides

$$\begin{bmatrix} d & a+ib\theta & 0 & i\theta c \\ i\theta g & d & 0 & 0 \\ 0 & i\theta r & d & e+i\theta s \\ 0 & 0 & i\theta g & d \end{bmatrix}\begin{bmatrix}\xi_{1,k}\\ \xi_{2,k}\\ \xi_{3,k}\\ \xi_{4,k}\end{bmatrix}= \tag{34}$$

$$\begin{bmatrix} d & a-i(1-\theta)b & 0 & -i(1-\theta)c \\ i(1-\theta)g & d & 0 & 0 \\ 0 & -i(1-\theta) & d & e-i(1-\theta)s \\ 0 & 0 & -i(1-\theta)g & d \end{bmatrix}\begin{bmatrix}\xi_{1,k}\\ \xi_{2,k}\\ \xi_{3,k}\\ \xi_{4,k}\end{bmatrix}$$

where

$$a=\frac{-2p}{h\Delta t}\cos mk\Delta x,\ b=\frac{-\left(\frac{p^2}{h^2}-gh\right)}{\Delta x}\sin mk\Delta x,$$

$$c=\frac{gh}{\Delta x}\sin mk\Delta x,\ d=\frac{1}{\Delta t},\ e=\frac{-2p_0}{h_0\Delta t}\cos mk\Delta x,$$

$$s=\frac{-\left(\frac{p_0^2}{h_0^2}-gh_0\right)}{\Delta x}\sin mk\Delta x,\ r=gh_0\frac{\lambda}{\Delta x}\sin mk\Delta x,$$

$$g=\frac{1}{\Delta x}\sin mk\Delta x,\ m=\frac{\pi}{(JJ-1)\Delta x}$$

and k denotes wave component. Then for the amplification factor, Φ, satisfying $\xi_{j,k}^{n+1}=\phi\xi_{j,k}^n$, the indeterminancy condition of determinant yields the quadratic equation

$$\left[1+\frac{g\theta^2}{d^2}(s+b)+\frac{g\theta^4}{d^3}(bs-rc)\right](\phi-1)^4$$

$$+\left[\frac{2\theta g}{d^2}(s+b)+\frac{4g^2\theta^3}{d^4}(bs-rc)\right](\phi-1)^3$$

$$\left[\frac{g}{d^2}(s+b)+\frac{6g^2\theta^2}{d^4}(bs-rc)\right](\phi-1)^2$$

$$\left[\frac{4g^2\theta}{d^4}(bs-rc)\right](\phi-1)+\frac{g^2}{d^4}(bs-rc)=0 \tag{35}$$

The equation can be solved numerically using the data to be used for the study of lock-exchange. The

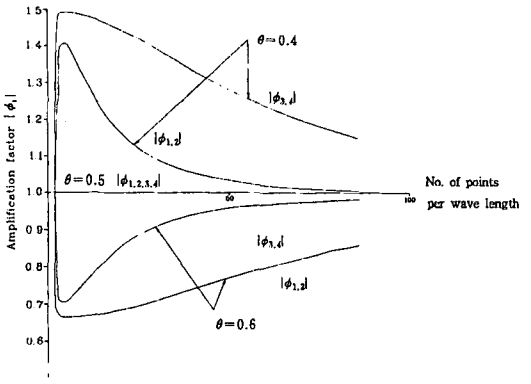

Fig. 3. Amplification portrait of scheme.

complex amplification factors consist of two pairs of complex number, each having its conjugate. The calculated result is plotted in case of Cr=8.0 in Fig. 3.

For $\theta = 0.5$ the result shows that this scheme has no amplification error. But for θ>0.5 the scheme is shown to be unconditionally stable and dissipative while the scheme is unstable for θ<0.5. This scheme is seen to be very effective to prevent the short wave from growing for 0.5, but damping effect even in relatively long components is shown to be severe for θ=0.6. For several conditions of θ and Courant number the results show that with caution against non linear energy transfer the choice of θ=0.5 gives the scheme optimum accuracy. The stability can be ascertained by showing that the energy norm is bounded through the simulation. Phase error can be also studied based on the form, that is, Q=-arctan(($Im(\Phi)/Re(\Phi)$)/2 Cr/Nx).

3.3 Solution Algorithm

In this section the solution method of the algebraic equation obtained in Section 3.2 is treated. As mentioned in introduction, the study is restricted to sub-subcritical flow case, in which case the double sweep algorithm is efficiently used to obtained solution. In the study of Abbott and Grubert (1972), the solution algorithm in the more general conditions had been studied.

The algebraic relation, for the solution of the scalar form of system (27), is suggested.

$$P_j = H_{j+1} h_{j+1} + I_{j+1} h_{0j+1} + J_{j+1} \tag{36}$$

$$P_{0j} = K_j P_j + L_j h_{j+1} + M_j \tag{37}$$

$$h_{0j} = N_{j+1} P_{0j+1} + Q_{j+1} P_{j+1} + R_{j+1} \tag{38}$$

$$h_j = S_j h_{0j} = T_j P_{0j+1} + U_j \tag{39}$$

Now using the equations of system (27) and the above four relation the recurrence relation of each coefficient can be obtained. The computation is made through, what is called, double sweep procedure. The first sweep is initiated from one boundary or the other boundary. From the species of the given boundary condition the initiation of appropriate coefficients is to be calculated during the first sweep procedure. Then from the other boundary condition of the other side the return sweep is initiated.

In case of transport-diffusion equation it can be solved by using simple vector double sweep method. Generally speaking, the transport-diffusion process will influence the dynamic process, and vise versa. So, the dynamic and transport-diffusion computation should be linked to connect two processes. This is usually attained through a form of multi staging that is called parallel running was not sufficiently appreciated due to the assumption of homogeneous flow in each layer, and the neglection of mixing. But through the experience the truncation error of transport-diffusion seems to grow as time elapses, meaning that more accurate scheme be employed to treat this effect in case long term simulation is required. When density is set to be constant in each layer, the transport-diffusion need not to be computed.

4. TESTS AND APPLICATIONS

To investigate the performance of the model the basic tests consisting of static and swing tests have been carried out. The model experiments have been carried out both for the lock-exchange flow and for the generation and propagation of internal tide over sharp bottom topography along with general applicability experiment for the condition of the downstream boundary conditions.

4.1 Static and Swing Tests

The testing of the computer program code for the

simulation of two layer flow is carried out. As a check of consistency of the mathematical model what is called, static and swing test are carried out.

To see the consistency of a mathematical model a test was carried out, using the initial data of uniform depth with each layer thickness 1 m as well as with zero initial velocity. No stress and horizontal bed condition were given. As a result of computation no change of depth happens and in case of momentum field no change of initial field was observed to the order of about 10^{-3} while a small deviation of about 10^{-4} order was observed. Until sufficient time steps the magnitude remains uniformly bounded. This result is sufficient to show that the model is quite good on the consistency.

As another check of consistency of the finite difference equation swing test is investigated. with a initial condition of uniform total depth and a linear slope of interface the test is carried out, as well as with the condition of zero initial momentum field at both layers. In this test time weighting, θ is chosen as 0.5 and no stress is included in equations. The response of internal and external mode is well represented as expected. The period of the internal mode is shown to be about 9 seconds with ρ/ρ_0=800/1100. The comparison of the results with the theoretical or experimental one is not made. The more comparison with field data is made in lock exchange experiment in the following section.

4.2 Application to Exchange Flow

The result of application of model to a lock exchange is given. The comparison of the simulated result with the laboratory result reported by Hodgins (1979) is made in four cases with each case having the result of the four different elapsed time steps. Each case is investigated to see the effects of time weighting, the coefficient of stresses, dissipative interface to the result of simulation, and finally to see the response of model with stress coefficient suggested by Hodgins.

Shortly is the experiment summarized that Hodgins carried out in a rectangular flume with dimension and initial configuration as shown in Fig. 4, as described in

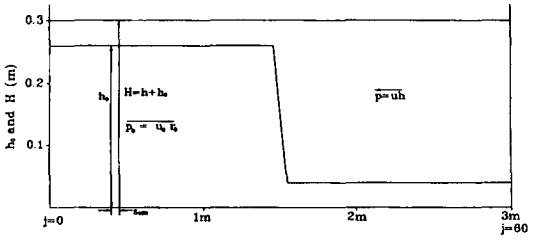

Fig. 4. Definition sketch of experiment.

his paper. The exchange flows were produced by quickly removing a thin barrier between the two fluids; the barrier was not vertical but at a inclination matched to the 5 cm grid spacing.

The free surface and interfacial positions of a number of exchange flows were recorded photographically using water dyed black and clear petroleum spirits as the two fluids. The object here was not to create a "discontinuous" front, but to obtain nearly that with thin layer on either side of the barrier. Then the mathematical model and its solution procedure are directly applicable. Each experiment was started by removing the barrier quickly, but smoothly, by hand. Optical distortion of the observation was by using two cameras, exposing simultaneously at regular intervals and timing controlled by including a clock in one photograph. The use of water soluble ink for dyeing the lower layer had the un expected advantage of creating a thin film of ink, particles on the free surface above the petroleum spirits and so rendering it highly visible. The value of t has an error of +0.2 s and the internal wave period is approximately 16 s. These tests have the advantage of being easily created and observed in the laboratory, and of severely testing the model response since the propagation of a large amplitude internal wave, at about the limiting resolution of the computational grid must be properly computed.

The physical parameter used in the simulation is

Table 1. Physical parameter of lock exchange experiment.

$\rho = 0.784 \pm 0.005$ g/ml	$\rho_0 = 1.001 \pm 0.0005$ g/ml
$g = 981.924$ cm/s^2	$j = 0,60$
Initial condition (shown in Fig. 4)	
$h_{j=0} = 2.63 \pm 0.05$ cm	$h_{j=60} = 22.50 \pm 0.05$ cm
$h_{0j=0} = 23.37 \pm 0.05$ cm	$h_{0j=60} = 3.50 \pm 0.05$ cm

Table 2. Comparison times of experimental and numerical ones.

exposure	experiment (s)	n (time steps)	elapsed time (s)
1	2.1±0.2	10	2.0
2	4.7±0.2	23	4.6
3	8.9±0.2	45	9.0
4	16.0±0.2	81	16.2

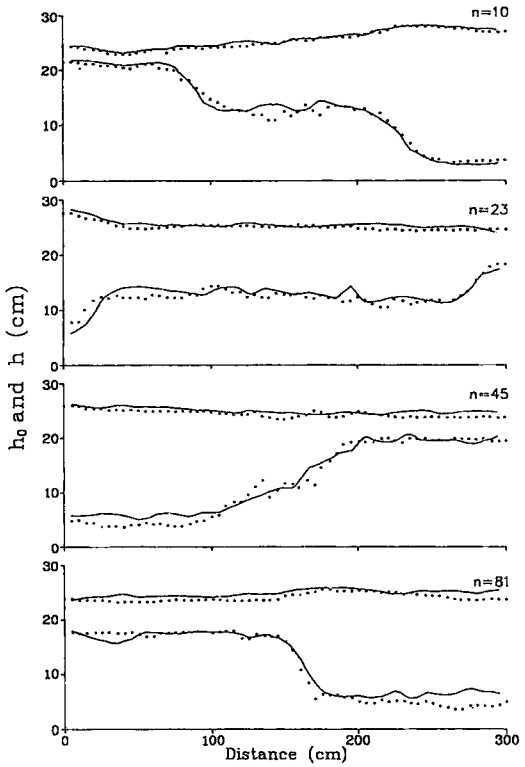

Fig. 5. Comparison of calculated levels(−) with observed ones(···) for $\theta = 0.5$, $K_i = 0.0004$ cm/s, K_b=0.0001.

listed in Table 2. Four times in each case of variable conditions is the numerical result compared with experimental results. Both the elapsed time and time steps to be compared are listed in Table 2.

Case 1:

In this case (θ=0.5) interfacial and bottom stresses are incorporated. And K_i equals 0.0004 cm^2/s and K_b equals 0.0001. Even though much attempt is not made to produce best agreement with the observed result, based on published values of coefficients for oscillating flows, the simulated result gives reasonable agreement with that observed. During the first cycle both the surface and long internal mode are well modelled, as

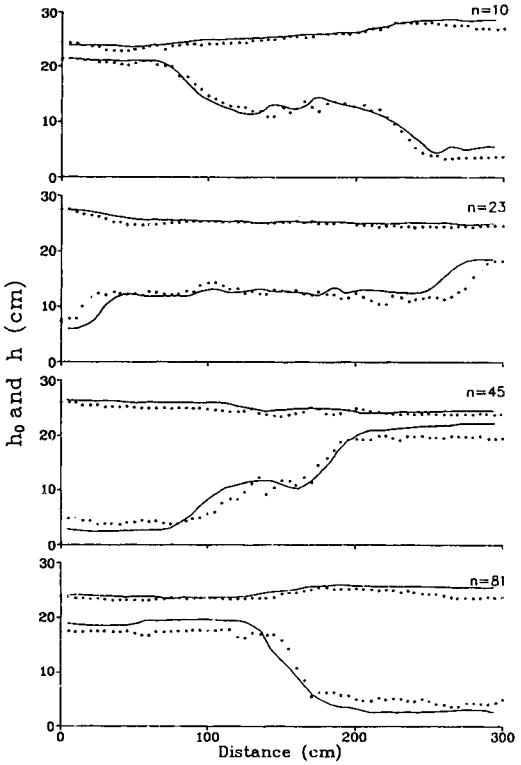

Fig. 6. Comparison of calculated levels(−) with observed ones(···) for $\theta = 0.6$, $K_i = 0.0$ cm/s, $K_b = \alpha = 0.0$.

shown in Fig. 5. The short internal mode superposed on the long internal mode is also relatively well simulated even though this mode is thought to be better simulated with more fine grid.

Case 2:

The response of model is tested with θ=0.6, but with stresses. In this case the general phase pattern of internal mode is also seen to be well simulated, as shown in Fig. 6. However, as expected from the characteristics of scheme, the dominant smoothing effect is observed with short internal waves effectively eliminated. In this case the pattern of two mode is almost coincident with that simulated by Hodgins, as expected. However, careful inspection of result shows that a slight phase delay or advance compared with that observed is shown and in spite of its preferential dissipation effect over short waves ranges a slightly low energy dissipation from the whole system is seen to be incorporated when we compare the simulated interface level with the

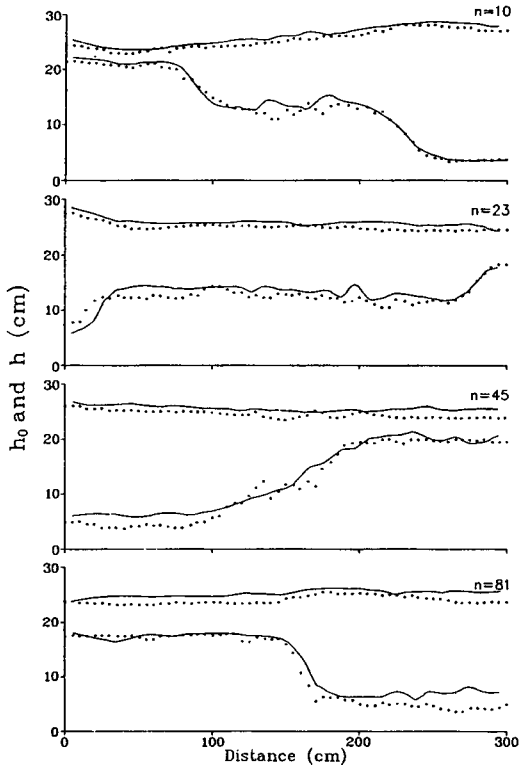

Fig. 7. Comparison of calculated levels(−) with observed ones(···) for $\theta = 0.5$, $K_i = 0.0$ cm/s, $K_b = 0.0004$, $\alpha = 0.075$.

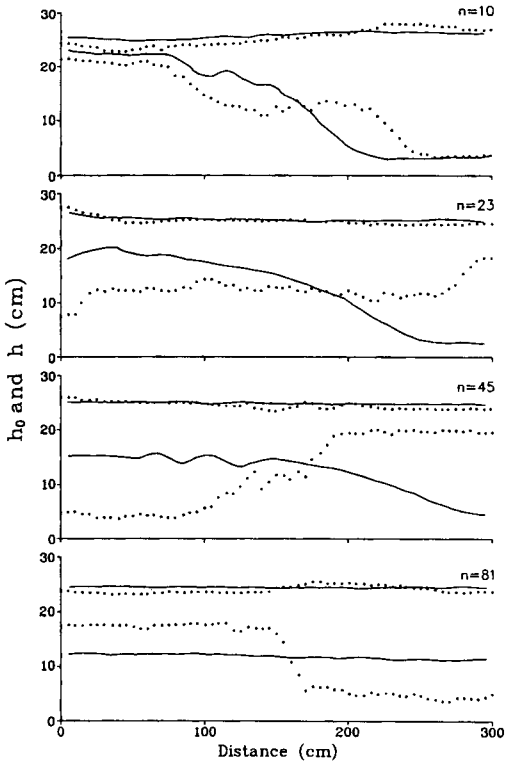

Fig. 8. Comparison of calculated levels(−) with observed ones(···) for $\theta = 0.5$, $K_i = 0.0008$ cm/s, $K_b = 0.0005$.

observed one at n=45 and n=81.

Case 3:

As examined by Hodgins, with dissipation term will the nonlinear instability in sufficient time steps happen in case of θ=0.5. In that case such instability could be avoided through the introduction of dissipative interface (Abbott, 1979) of the form wi'. constant α

$$f = f_j^n + \alpha[f_{j+1}^n - 2f_j^n + f_{j-1}^n]$$

With both dissipative and bottom stress an investigation is made. The overall shape of the internal mode, shown in Fig. 7, is seen to be well simulated through the one cycle. The attempt to use only dissipative interface is not made.

Case 4:

Through the study by Hodgins (1979), the interfacial stress coefficient is chosen K_i=0.008 cm^2/s to give the result a reasonable agreement with observed one with fixed valued of K_b=0.005. Even though both longitudinal stress and lateral stress are included in his calculation as a form of $\tau_s = K_s u|u|$ *or* $\tau_s = K_s u_0|u_0|$ with $K_s = 0.01$. An attempt is made to investigate the response of model without this term. As shown in Fig. 8, the phase and amplitude pattern are greatly deviated from that obtained by Hodgins in case of θ=0.6. This response could be partly or wholly explained by the neglection of lateral and longitudinal stresses.

4.3 Application to Internal Tide

The internal tide is well known to exist in the continental shelf break. The layer model is considered as one of useful tools to investigate the generation and propagation in such a region. Even though Coriolis force is neglected in one dimensional two layer model, the basic characteristics of generation and propagation of internal tide would be sufficiently investigated using present model. In this application the adaptation of bottom topography and open boundary conditions at

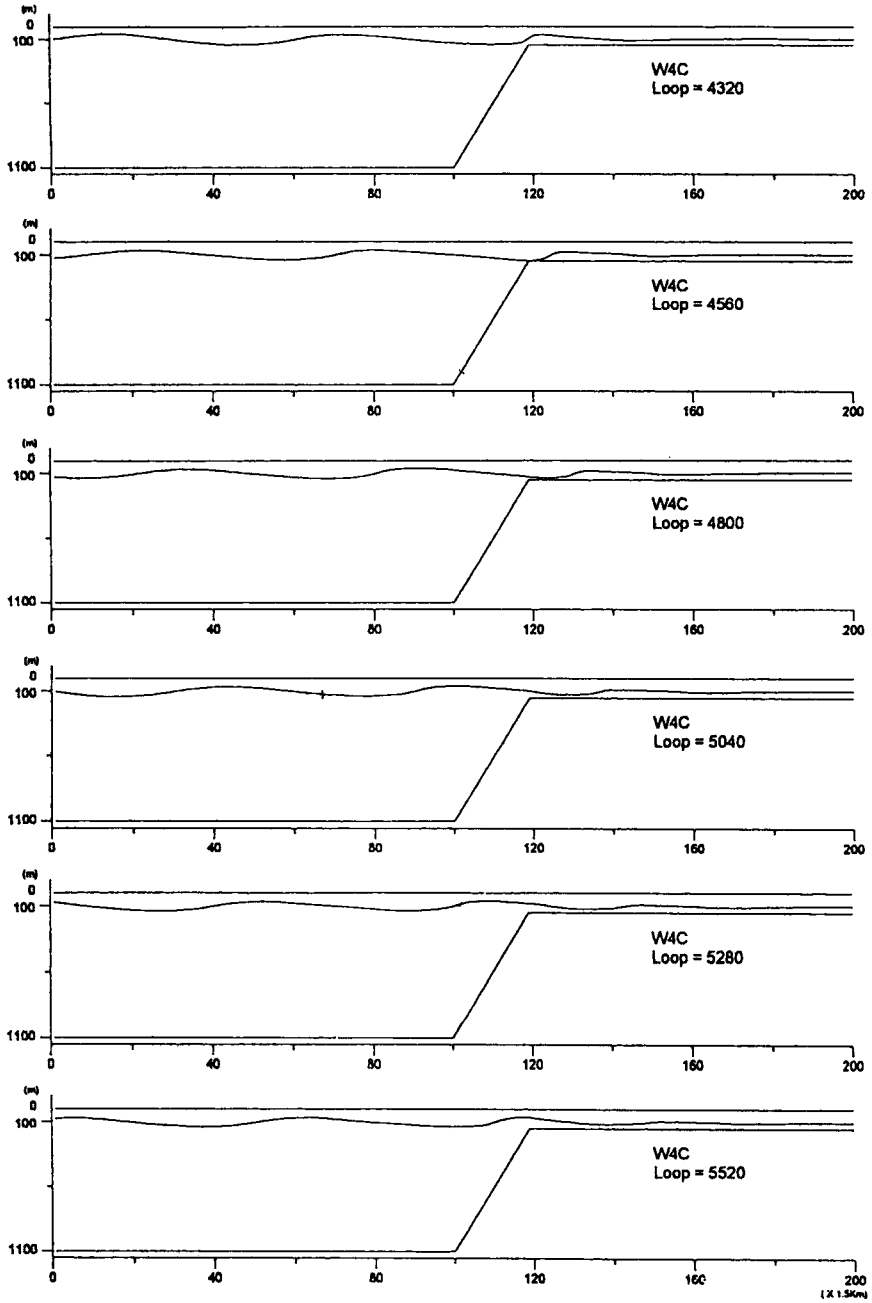

Fig. 9. Computed temporal variation of interfacial disturbance at the shallow downstream region of $h_o = 50$ m and $h = 100$ m. The amplitude of interfacial disturbance is exaggerated 10 times for visual effect. Following figures are samely exaggerated.

downstream channel are further considered in addition to simple basin study in previous application.

An experiment was first carried out to investigate the response of radiational boundary conditions at both the upper and lower layers in the downstream channel. The coefficients of K_i=0.0004, K_b=0.0001 and α=0.075 were used for this experiment. The densities of upper and lower layers are set to be 1021 and 1026 kg/m^3, respectively, which are characteristic values during summer in the shelf break of the East China Sea (Lie, 1995). The

left forcing boundary condition is as follows.

upper layer: $Q = A\cos(\omega t - \theta)$, $A = 10.0\ \mathrm{m}^2/s$, $\theta = 90^\circ$, $\omega = 2\pi/T$ with $T = 12$ hr

lower layer: $Q = 0.0$

The right open boundary condition of channel is as follows.

upper layer: $\frac{\partial \phi}{\partial t} + C\frac{\partial \phi}{\partial x} = 0$, $C = \sqrt{g(h + h_o)}$

lower layer: $Q = 0.0$ or $\frac{\partial \phi}{\partial t} + C\frac{\partial \phi}{\partial x} = 0$,

$$C = \sqrt{\frac{g(1-\lambda)hh_0}{h + h_0}}$$

where variable ϕ denotes mass flux, h and h_o the thickness of upper and lower layers, respectively. The h and h_o in the upstream region from left boundary to 150 km are 100 and 1,000 m, respectively, while those in the upstream region from right boundary to 120 km are h_0=50 m, H=100 m. The grid interval is 1.5 km and computation time interval (dt) is 30 s. In case of right open boundary condition the radiational condition at both layers may be used. However, the results with Q= 0.0 at lower boundary shows similar results to the results using radiation condition. This may be due to the transfer of minor energy since the channel length of downstream part of channel is relatively long.

The computed every 2 hour variations of interface and free surface with the downstream thickness of h_0= 50 m, h=100 m are presented in Fig. 9. The variation of interface was 10 times exaggerated for visual effect. It is shown that the propagation features of internal wave from upstream to downstream channel is well simulated, confirming the applicability of two types of boundary conditions. Considering the propagation features both in downstream and upstream channels, it is seen that the internal wave in the shallow downstream seem to show severely damped oscillation. This experiment helps us examine the variation pattern of incident internal wave over the sharp bottom topography and investigate if radiational boundary condition works.

The experiments with different lower layer thickness were designed in order to investigate the generation effect of internal tidal wave only in the downstream. The depth in upstream channel was set to be 120 m, and 200 m in the downstream, since lower layer thickness was. The results with h_0=100 m and h=100 m at the downstream channel are shown in Fig. 10. Fig. 11 is the result with downstream channel thickness of h_0= 20 m and h=100 m. In both experiments the layer thicknesses in the upstream region are h_0=20 m and h=100 m, while those in the middle channel are h_0=1000 m and h=100 m. In Figs. 10 and 11 the generation effect in the shallow upstream region seems to be largely reduced. However, the generation of internal tide in the upstream shelf break region appears clearly.

It is also seen that the internal wave in case of downstream thickness h_0=100 m propagates more actively through the downstream boundary, compared with the case of downstream thickness h_0=20 m. That is, the magnitude of interfacial wave disturbance in the downstream region of Fig. 10 appears larger than that in Fig. 11. It can be said that the energy transfer occurs more actively with increasing thickness of lower layer in the downstream. This result suggests that the internal tidal wave can only propagate for the condition greater than some critical lower layer thickness, also implying that the propagation of internal wave will be limited if the thickness of lower layer is very thin.

The seasonally varying layer thickness often revealed from the density structure in the shelf break, such as that in the East China Sea, implies that the tidal signal in the interfacial disturbance will show corresponding changes. The internal oscillation induced by internal tide will be extremely restricted for the season when barotropic feature over the water column prevails.

The additional experiments seem to be required only in order to examine the generation effect in the downstream shelf break region. Lamb(1994) used a model based upon rigid lid assumption in quasi 3-dimensional numerical experiment for the George Bank. He was able to treat the upstream and downstream boundary conditions more easily only by introducing barotropic components at both upstream and downstream boun-

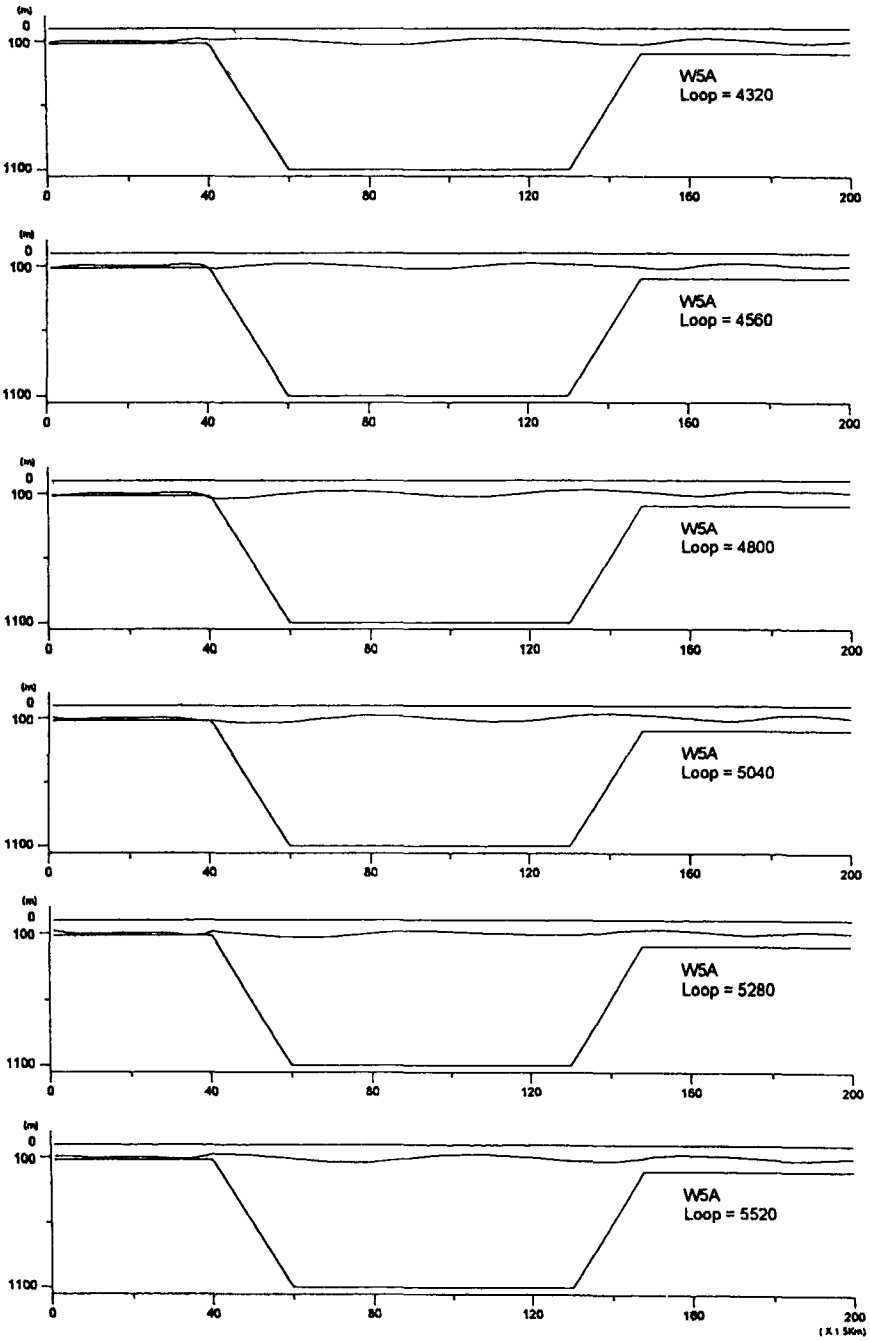

Fig. 10. Same as in Fig. 9 except for at the shallow downstream region of $h_o = 100$ m and $h = 100$ m.

dary. In future more flexible approaches may be examined in order to investigate the generation effect over shelf break, even though the shallow thickness of lower layer in layer model was shown to be useful for such purpose.

5. DISCUSSIONS AND CONCLUSIONS

The numerical implicit finite difference scheme described by Abbott and Ionescu is shown to be successfully applied to the simulation of two layer depth avera-

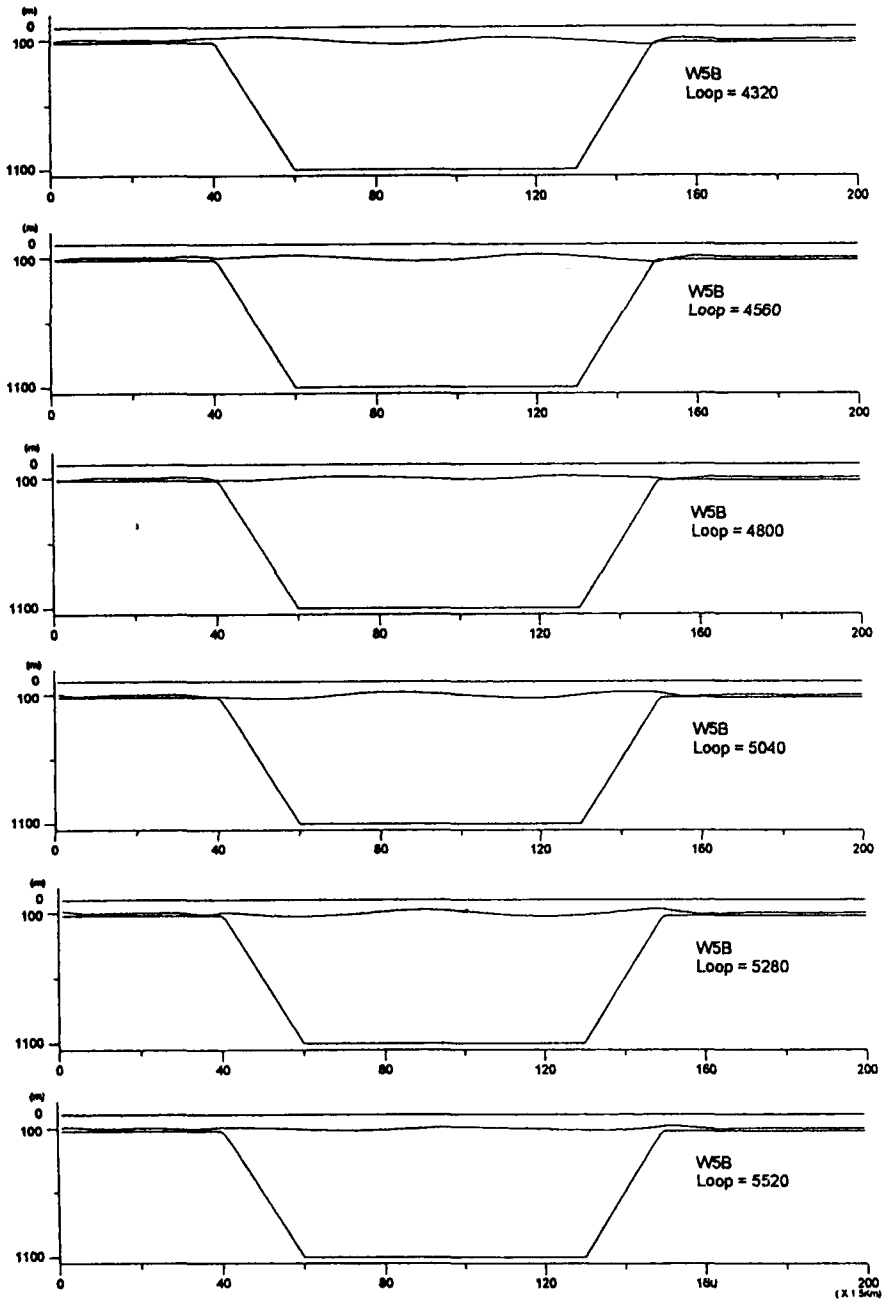

Fig. 11. Same as in Fig. 9 except for at the shallow downstream region $h_0 = 20$ m and $h = 100$ m.

ged governing equations. The numerical exchange test shows that the internal and external modes, both in phase and amplitude, can be accurately simulated over the relatively large time increment compared with explicit scheme. And the dissipative characteristics of scheme for time weighting factor θ<0.5 could be used to eliminate the short wave causing the instability to possibly occur after sufficient time. When long term simulation is required, the dissipative interface with θ= 0.5 could be effectively applied for numerical stability. Through the several case studies of lock exchange flow the result of model is shown to work reasonably, and

so possibly applied to the simulation of practical situation.

Two-layer model experiment has been also carried out to investigate the generation and propagation characteristics of internal tidal wave over the steep bottom topography under stratified condition. The internal wave seems to well radiate through the downstream boundary under the experiments adopting radiation conditions both at two layers and only at upper layer, confirming the applicability of two types of boundary conditions. It is shown that the energy transfer occurs more actively with increasing thickness of lower layer in the downstream. This result suggests that the internal tidal wave can only propagate for the condition greater than some critical lower layer thickness, also implying that the propagation of internal wave will be limited if the thickness of lower layer is very thin.

ACKNOWLEDGEMENTS

The main part of this study was carried out during S. K. Kang's participation in the course of International Institute for Hydraulic and Environmental Engineering (IHE), Delft, The Netherlands. A sincere thanks goes to T. Minns and A. Verwey for their kind discussions, comments, and lectures. A special thanks go to the staffs of computer operating group for their kind help through this work. Partial support in the field application to internal tide was provided by the Korea Ministry of Science and Technology through Grant BSPN 00278-901-1.

REFERENCES

Abbott, M.B., 1961. On the spreading of one fluid over another, *La Houille Blanche*, **16** (5 and 6), pp. 622-635 and 827-846.

Abbott, M.B., 1963. On flows and fronts in a stratified fluid, *Proc. Royal Society*, A, **273**, pp. 12-40.

Abbott, M.B. and Ionescu, F., 1967. On the numerical computation of nearly-horizontal flows, *J. Hyd. Res.*, **5**(2), pp. 97-117.

Abbott, M.B., Bertelsen, J.A., Kej and Warren, I.R., 1975. Systems modelling of stratified fluids, *Proc. XVI Congress of the IAHR*, Sao Paulo, 1975.

Abbott, M.B. and Grubert, J.P., 1972. Numerical computation of stratified nearly-horizontal flows. *J. Hyd. Div.*, ASCE, **HY10**, pp. 1847-1865.

Abbott, M.B., 1979. *Computational hydraulics: elements of the theory of free surface flows*, Longman, London.

Abraham, G. and Eysink, W.D., 1971. Magnitude of interfacial shear in exchange flow, *J. Hyd. Res.*, **9**(2), pp. 125-132.

Abraham, G., 1982-1983. Reference notes on density current and transport process.

Delft Hydraulic Laboratory, 1979. Computation of density currents in estuaries, Report on mathematical investigation, R 897 Part IV.

Ellison, T.H. and Turner, J.S., 1959. Entrainment in stratified flows, *J. Fluid Mech.*, **6**, pp. 423-448.

Hyden, H., 1974. Water exchange in two-layer stratified waters, *J. Hyd. Div.*, ASCE, **HY3**, pp. 345-361.

Hodgins, D.O., 1979. On the numerical computation on two-layer nearly horizontal flows, *J. Hyd. Res.*

Lax, P.D. and Wendroff, B., 1960. System of conservation laws, *Comm. Pure and Applied Math.*, **13**, pp. 217-237.

Lie, H.J., 1995. Ocean circulation and material flux of the East China Sea (First year), Korea Ocean Res. and Dev. Inst., Rep. No. BSPN 00257-812-1 (in Korean).

Vreugdenhil, C.B., 1970. Two-layer model of stratified flow in an estuary, *La Houille Blonche*, **1**, pp. 35-40.